

## Dynamical properties of copper halides. II. Theoretical study of the anomalies in the line shape of the transverse optic phonons

G. Kanellis,\* W. Kress, and H. Bilz

*Max-Planck-Institut für Festkörperforschung, Heisenbergstrasse 1, 7000 Stuttgart 80, Federal Republic of Germany*

(Received 11 November 1985)

The anomalous line shapes of the transverse optic (TO) phonons of the copper halides CuCl, CuBr, and CuI observed in Raman and neutron scattering experiments are calculated in the framework of valence-shell models, which are extended to include the leading third-order anharmonic terms. The self-energies of the zone-center TO modes are calculated and it is shown that the anomalous line shapes are due to Fermi resonances. The good agreement between the calculated and the measured line shapes shows that other explanations such as two-phonon bound states and off-center ions can be ruled out.

### I. INTRODUCTION

The anomalous line shapes of the transverse optic (TO) phonons of the copper halides CuCl, CuBr, and CuI have attracted considerable interest in recent years both experimentally and theoretically.

The first-order Raman spectra of CuCl reveal a pronounced double- and sometimes even triple-peak structure at about the frequency of the  $\text{TO}(\Gamma)$  phonon.<sup>1-13</sup> This structure is an inherent phonon property, which has also been observed in inelastic neutron scattering experiments at low temperature.<sup>14</sup> The neutron scattering measurements not only reveal the double-peak structure of the  $\text{TO}(\Gamma)$  phonon, but also show that the TO-phonon spectrum is strongly wave-vector dependent and turns progressively into a normal quasi-harmonic mode spectrum when the frequency of the TO phonon is increased by increasing the wave vector. This behavior indicates strongly that the anomalous line shape is due to a resonance phenomenon. The pressure dependence of the line shapes points in the same direction. Pressure-dependent first-order Raman scattering measurements reveal important changes in the line shapes.<sup>10-12</sup> At low pressures the line shape is changed and a small third peak shows up. With further increasing pressure up to the phase transition, the intensity and the frequency of the lower-frequency peak decrease monotonically.

Similar features are observed also in the first-order Raman spectra of CuBr.<sup>10-12</sup> At very low temperatures the  $\text{TO}(\Gamma)$  mode has a single-peak structure. At moderate temperatures a second low-intensity peak shows up at the low-frequency side of the TO mode. With increasing pressure, this peak increases in intensity and broadens considerably so that close to the phase transition only one very broad structure is observed.

The Raman spectrum of CuI does not display any particular features except for a significant broadening at higher temperatures and pressures.<sup>15</sup>

Much interest has been devoted to the explanation of the anomalous line shapes observed in CuCl. The early explanations of the Raman spectra by a superposition of

first- and second-order spectra<sup>7</sup> have been ruled out experimentally<sup>5</sup> and the spectra have been confirmed to be of first order.<sup>14</sup> Krauzman *et al.*<sup>8</sup> attributed the double-peak structure in the first-order Raman spectra of CuCl to a Fermi resonance between the  $\text{TO}(\Gamma)$  mode and the two-phonon density of states. They approximated the two-phonon bands of the optic modes by an elliptically shaped density function, which contained one adjustable parameter and made use of an earlier suggestion by Ruvalds and Zawadowski,<sup>16</sup> according to which weak fourth-order anharmonic terms in the potential give rise to resonances near the upper cutoff frequency of the two-phonon bands while a two-phonon bound state may be formed above the cutoff frequency, when the fourth order anharmonic terms become sufficiently strong. Resonances or bound states may interact through third-order terms in the potential with the one-phonon states. As a result, double-peak structures can be obtained for a certain range of anharmonic interactions. Using this model Krauzman *et al.*<sup>8</sup> and Shand *et al.*<sup>17</sup> described the Raman spectra of CuCl. Both calculations were based on a model two-phonon density of states of elliptical shape. No use was made of a detailed model description of the phonon dispersion curves from which the two-phonon summation and difference bands can be obtained. In both calculations the disposable parameters which described the anharmonic interactions, as well as the shape of the two-phonon density of states, were fitted to the measured line shapes.

A similar procedure has been followed by Hennion *et al.*<sup>14</sup> in their analysis of the neutron data for CuCl. Here again all disposable parameters were fitted to the observed line shapes. It should be mentioned here that the relative intensities of the two peaks observed in CuCl seem to be to some extent sample dependent and that in some spectra a small third peak shows up in between the two main peaks. Yet another small peak has been observed at  $60 \text{ cm}^{-1}$ .<sup>3,6,9,13</sup> These additional peaks cannot be explained by the models mentioned above.

Vardeny and Brafman<sup>13</sup> propose a completely different model to explain the anomalous line shapes observed in copper halides. They consider a disorder model in which

the  $\text{Cu}^+$  ions may occupy their lattice positions as well as four equivalent off-center positions in the directions of the four nearest-neighbor bonds. The  $\text{Cu}^+$  ions are allowed to tunnel between these positions. The authors claim that the system can be treated in the long-wavelength limit as a mixed crystal which shows a two-mode behavior. The two TO modes of the mixed crystal give rise to the double-peak structure. The small third peak between the two TO peaks is considered as one of the LO modes of the two-mode system.

We show in this paper that the observed line shapes of all three copper halides can be calculated on the basis of phenomenological models for the lattice dynamics which have been presented in the first paper (hereafter called I) of this series.<sup>18</sup> With these models we calculate the appropriate two-phonon densities of states for sum and difference processes and show that the observed line shapes are in fact due to a Fermi resonance of the  $\text{TO}(\Gamma)$  modes with the two-phonon densities of states. In our calculation we take into account the leading term in the third-order expansion of the short-range potential for the coupling between the  $\text{TO}(\Gamma)$  mode and the two-phonon density. We show that the line shapes are to a large extent determined by the high-density parts in the two-phonon spectrum and their position relative to the  $\text{TO}(\Gamma)$  frequency. Thus the changes in both the two-phonon densities and the relative position of the TO modes explain the differences in the line shapes of the three copper halides. This study was highly motivated by the new experimental data obtained by Blacha<sup>11</sup> and Blacha *et al.*<sup>12</sup>

In Sec. II we outline the anharmonic theory used in this study. The numerical results are presented in Sec. III.

## II. THEORY

In order to account for anharmonic effects, the harmonic models used to fit the experimental phonon dispersion curves are extended to include third- and fourth-order anharmonic terms in the expansion of the potential. The anharmonic part of the Hamiltonian is written as

$$H_A = \sum_{\lambda_1, \lambda_2, \lambda_3} V^{(3)}(\lambda_1, \lambda_2, \lambda_3) A_{\lambda_1} A_{\lambda_2} A_{\lambda_3} + \sum_{\lambda_1, \lambda_2, \lambda_3, \lambda_4} V^{(4)}(\lambda_1, \lambda_2, \lambda_3, \lambda_4) A_{\lambda_1} A_{\lambda_2} A_{\lambda_3} A_{\lambda_4}, \quad (1)$$

where  $\lambda_i$  is a combined index for the wave vector  $\mathbf{q}_i$  and the branch index  $j_i$ , which label the phonon  $i$ . The phonon field operators  $A_\lambda$  are defined in terms of phonon creation ( $a_\lambda^\dagger$ ) and annihilation ( $a_\lambda$ ) operators by the relations

$$A_\lambda = a_{-\lambda}^\dagger + a_\lambda, \quad A_\lambda^\dagger = a_\lambda^\dagger + a_{-\lambda} \quad (2)$$

and the expansion coefficients  $V^{(3)}$  and  $V^{(4)}$  are related to the Fourier transforms  $\phi^{(3)}(\lambda_1, \lambda_2, \lambda_3)$  and  $\phi^{(4)}(\lambda_1, \lambda_2, \lambda_3, \lambda_4)$  of the third- and fourth-order anharmonic expansion coefficients of the interaction potential with respect to the atomic displacements by the relations<sup>19</sup>

$$V^{(3)}(\lambda_1, \lambda_2, \lambda_3) = \frac{1}{3!} \left[ \frac{\hbar}{2} \right]^{3/2} N^{-1/2} (\omega_{\lambda_1} \omega_{\lambda_2} \omega_{\lambda_3})^{-1/2} \times \phi^{(3)}(\lambda_1, \lambda_2, \lambda_3) \Delta(\mathbf{q}_1 + \mathbf{q}_2 + \mathbf{q}_3) \quad (3)$$

and

$$V^{(4)}(\lambda_1, \lambda_2, \lambda_3, \lambda_4) = \frac{1}{4!} \left[ \frac{\hbar}{2} \right]^2 N^{-1} (\omega_{\lambda_1} \omega_{\lambda_2} \omega_{\lambda_3} \omega_{\lambda_4})^{-1/2} \times \phi^{(4)}(\lambda_1, \lambda_2, \lambda_3, \lambda_4) \Delta(\mathbf{q}_1 + \mathbf{q}_2 + \mathbf{q}_3 + \mathbf{q}_4),$$

where  $\omega_{\lambda_i}$  are the eigenfrequencies in the harmonic approximation and  $\Delta(\sum_i \mathbf{q}_i)$  is the generalized  $\delta$  function, which is unity for  $\sum_i \mathbf{q}_i$  equal to zero or a reciprocal-lattice vector and zero otherwise. It has been pointed out by Oitmaa<sup>20</sup> that the Hamiltonian of a shell model does not only contain anharmonic terms in the displacements of the centers of the ionic masses (ionic displacements) but also cubic and higher-order terms in the relative displacements of the shell with respect to the core displacements as well as mixed terms in the displacements of the cores and the relative displacements of the shells. These contributions renormalize the anharmonic terms in the ionic displacements. In the harmonic approximation the contributions from the relative shell displacements renormalize the rigid-ion frequencies by less than about 10–20%. The renormalization of rigid-ion frequencies can, however, be much larger, when the electron-phonon interaction is strong and leads to pronounced anomalies in the phonon dispersion curves (e.g., in refractory compounds<sup>21</sup>) or to ferroelectric soft modes.<sup>22,23</sup>

In copper halides such anomalies do not occur. Since we are interested here in the leading terms, we neglect the small renormalization of the anharmonic terms in the ionic displacements by the anharmonic contributions from the relative core-shell displacements. Thus we consider only an effective anharmonic potential for the ionic displacements and write the third-order anharmonic potential as

$$\phi^{(3)}(\lambda_1, \lambda_2, \lambda_3) = \sum_{l', l''} \sum_{\kappa, \kappa', \kappa''} \sum_{\alpha, \beta, \gamma} \phi_{\alpha\beta\gamma}(0, \kappa; l', \kappa'; l'', \kappa'') e_\alpha(\kappa, \lambda_1) e_\beta(\kappa', \lambda_2) e_\gamma(\kappa'', \lambda_3) e^{iq[\tau(l') - \tau(l'')]}, \quad (4)$$

where  $\phi_{\alpha\beta\gamma}(0, \kappa; l', \kappa'; l'', \kappa'')$  is the third-order anharmonic interaction matrix and  $e_\alpha(\kappa, \lambda_i)$  is the component  $\alpha$  ( $\alpha = x, y, z$ ) of the eigenvector of the ion  $\kappa$  in the mode  $\lambda_i$ . The fourth-order term is given by an analogous expression.

From the anharmonic terms  $\phi^{(3)}$  and  $\phi^{(4)}$  the phonon self-energy  $\Sigma(\lambda, \omega)$  is calculated taking into account the lowest-order diagrams given in Fig. 1.

In this approximation the phonon self-energy

$$\Sigma(\lambda, \omega) = (\hbar/kT) [\Delta(\lambda, \omega) - i\Gamma(\lambda, \omega)] \quad (5)$$

reads

$$\begin{aligned} \Sigma(\lambda, \omega) = & \Sigma_0 + 12 \sum_{\lambda_1} V^{(4)}(\lambda, -\lambda, \lambda_1, -\lambda_1) [2n(\omega_1) + 1] - 36 \sum_{\lambda_1, j'} V^{(3)}(\lambda_1, -\lambda_1, j') V^{(3)}(j', \lambda_1, -\lambda_1) [2n(\omega_1) + 1] / \omega(j') \\ & + \frac{18}{\hbar k T} \sum_{\lambda_1, \lambda_2} |V^{(3)}(-\lambda, \lambda_1, \lambda_2)|^2 R(\lambda_1, \lambda_2, \omega), \end{aligned} \quad (6)$$

with

$$\begin{aligned} R(\lambda_1, \lambda_2, \omega) = & \frac{n(\omega_1) + n(\omega_2) + 1}{\omega_1 + \omega_2 + \omega + i\epsilon} + \frac{n(\omega_1) + n(\omega_2) + 1}{\omega_1 + \omega_2 - \omega - i\epsilon} \\ & + \frac{n(\omega_1) - n(\omega_2)}{\omega_2 - \omega_1 - \omega - i\epsilon} + \frac{n(\omega_1) - n(\omega_2)}{\omega_2 - \omega_1 + \omega + i\epsilon}, \end{aligned} \quad (7)$$

where  $k$  is the Boltzmann constant,  $\Delta(\lambda, \omega)$  and  $\Gamma(\lambda, \omega)$  are the frequency-dependent shift and linewidth of the mode  $\lambda$ , respectively,  $\omega_1$  and  $\omega_2$  are the harmonic phonon frequencies of the modes  $\lambda_1$  and  $\lambda_2$ , respectively, and  $j'$  is the branch index of the optic modes at  $\Gamma$ . The thermal occupation factor  $n(\omega)$  is

$$n(\omega) = 1 / [\exp(\hbar\omega/kT) - 1]. \quad (8)$$

The first two and the two last terms in Eq. (7) account for summation and difference processes, respectively. The first term in Eq. (6) is a real, frequency-independent contribution, which takes into account the frequency shift  $\Delta_0$  due to the thermal expansion of the lattice. The remaining three terms in Eq. (6) are the contributions due to Figs. 1(a), 1(b), and 1(c), respectively. The first two diagrams contribute only to a frequency-independent shift, whereas the third one describes the linewidth and shift of a phonon due to its decay into two phonon states.

Since the harmonic frequencies  $\omega_i$  which enter into equations (3)–(7) are not the quasiharmonic frequencies determined from the measured phonon dispersion curves, we use the self-consistent method of Fischer<sup>24</sup> to calculate the self-energy  $\Sigma(\lambda, \omega)$ . The phonon frequencies calculated with the shell model at finite temperature are quasiharmonic frequencies. They contain the shifts due to the anharmonic interactions but have still infinite lifetimes, i.e., no linewidths. These quasiharmonic frequencies are given by

$$\omega_i = [\omega_{0i}^2 + 2\omega_{0i}\Delta(\lambda_i, \omega_i)]^{1/2}, \quad (9)$$

where  $\omega_{0i}$  are the harmonic frequencies.

In the self-consistent approximations the infinitesimally

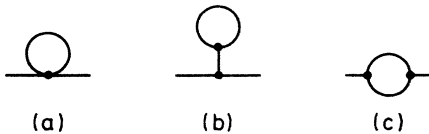


FIG. 1. Diagrams of the lowest-order contributions to the phonon self-energies.

small constant  $\epsilon \rightarrow 0^+$  in Eq. (7) is replaced by a finite damping constant  $\gamma$ , which is in a first approximation given by

$$\gamma = \gamma_1 + \gamma_2, \quad (10)$$

where  $\gamma_i$  is assumed to be proportional to  $\Gamma(\lambda, \omega_i)$  calculated in solving Eq. (6) self-consistently. The self-consistent procedure yields a solution of the Dyson equation with renormalized one-phonon propagators. Finally, the anharmonic line shape of the TO( $\Gamma$ ) phonon  $\omega(\lambda)$  is calculated from the relation

$$I(\lambda, \omega) = \frac{\Gamma(\lambda, \omega)}{[\omega(\lambda) + \Delta(\lambda, \omega) - \omega]^2 + \Gamma^2(\lambda, \omega)} [n(\omega) + 1]. \quad (11)$$

The calculations are based on the quasiharmonic frequencies obtained from valence-shell models described in I. The frequency-independent shift resulting from the first three terms in Eq. (6) is taken into account by a small adjustable constant  $\Delta_0$ . The important terms for the line shape of the TO( $\Gamma$ ) mode are those resulting from the three-phonon processes in Fig. 1(c). This diagram is taken into account in the leading-term approximation for the third-order contributions to the effective potential considering only the bond-stretching interaction,

$$\phi_{\text{anh}} = \frac{\lambda'}{6} \sum_{1-2} \Delta r_1^3, \quad (12)$$

where  $\lambda'$  is the third-order coupling constant and  $\Delta r_1$  is the change in the nearest-neighbor distance. The sum runs over all nearest-neighbor anion-cation pairs (1-2). The anharmonic bond-stretching force constant  $\lambda'$  not only accounts for the anharmonic short-range overlap contribution but also contains the anharmonicity of the strong nearest-neighbor Coulomb interaction. In view of the partial covalent character of the zinc-blende structure compounds and in view of the fact that the interplanar Coulomb force constants decrease rapidly with increasing interplanar distances, all other Coulomb contributions are neglected in the present calculation. The strength of the anharmonic coupling parameter  $\lambda'$  is adjusted as to obtain a best fit of the measured line shapes.

### III. RESULTS AND DISCUSSION

Following the procedure outlined in the preceding section, we calculate the self-energies and the line shapes of the TO( $\Gamma$ ) modes for CuCl, CuBr, and CuI.

Figure 2 shows the line shape of the TO( $\Gamma$ ) phonon for CuCl (solid curve) calculated with the valence-overlap-shell model. The experimental data of Krauzman *et al.*<sup>8</sup> are represented by the dashed curve. The agreement be-

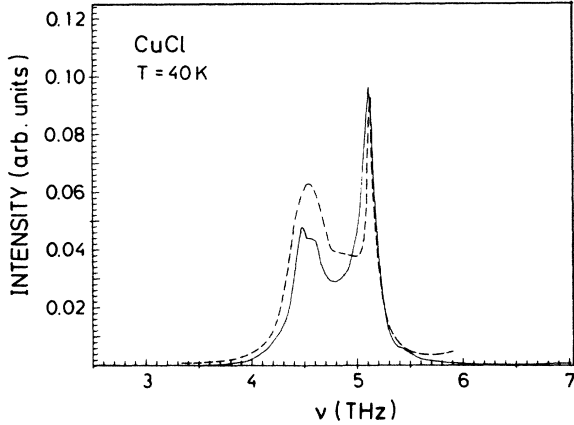


FIG. 2. Line shape of the  $\text{TO}(\Gamma)$  phonon in CuCl at 40 K calculated with the valence-overlap-shell model (VOSM) (solid curve). The dashed curve shows the experimental spectra of Krauzman *et al.* (Ref. 8). Anharmonic parameters are  $\lambda' = 16e^2/r_0v_a$ ,  $\Delta_0 = 0.2$  THz.

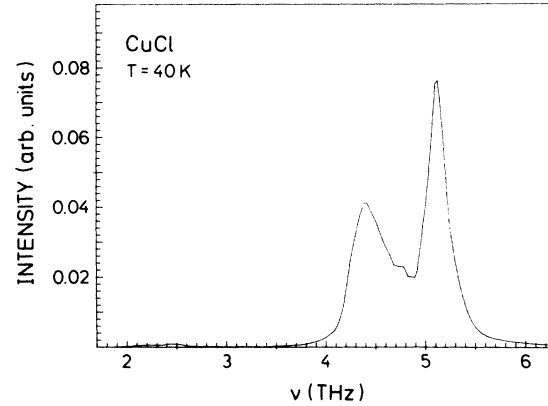


FIG. 3. Line shape of the  $\text{TO}(\Gamma)$  phonon in CuCl at 40 K calculated with a simple-valence-shell model (VSM). Note the third peak at about 4.75-THz. The small peak between 2 and 2.5 THz has also been observed in some Raman scattering experiments (Refs. 3, 6, 9, and 13). Anharmonic parameters are  $\lambda' = 26e^2/r_0v_a$ ,  $\Delta_0 = 0.4$  THz.

tween the calculated and measured line shape is gratifying. The close similarity between the two curves indicates that the observed anomalous line shape of the  $\text{TO}(\Gamma)$  phonon is indeed caused by a Fermi resonance between the  $\text{TO}(\Gamma)$  phonon and the two-phonon density of states. Our results show further that it is sufficient to take into account the leading term of the third-order anharmonic contributions to the three-phonon coupling processes. In our study we use the different models discussed in (I) to calculate the two-phonon densities of states. We find that all models yield nearly identical densities of states. The line shapes of the  $\text{TO}(\Gamma)$  phonons can also be reproduced by all these models rather accurately using different values of the anharmonic parameters. These differences are attributed to the different ways in which short-range and deformation contributions are separated in these models.

It should be pointed out here that the parameter  $\lambda'$  is not a pure scaling factor for the anharmonic coupling as could be expected from the structure of Eq. (6), but that it also influences the frequency dependence of the phonon self-energy via the self-consistency condition for the phonon linewidths. Thus an increase in  $\lambda'$  not only leads to larger values of  $\Gamma(\lambda, \omega)$ , but it also broadens the structures observed in  $\Gamma(\lambda, \omega)$ . It should be emphasized that the line shape of the  $\text{TO}(\Gamma)$  phonon depends to some extent on the wave vector of the incident light. This wave vector is so small that its effects on the phonon frequency can be neglected. The eigenvectors are, however, strongly dependent on the direction of  $\mathbf{q}$  even for small wave vectors. Since the experimental conditions under which the spectra have been obtained are not very clear with respect to the orientation of the samples, we have calculated the line shapes by averaging over different orientations. It should, however, be mentioned that the small differences observed in the measured spectra may be caused by different sample orientations with respect to the incident light. In Fig. 3 we represent the  $\text{TO}(\Gamma)$  line shape of CuCl obtained from a simple-valence-shell model.

The calculated line shape for the  $\text{TO}(\Gamma)$  phonon in

CuBr is shown in Fig. 4. This spectrum shows a main peak at about 4 THz and a pronounced shoulder extending to lower frequencies. Unfortunately, no detailed experimental data exist for CuBr at atmospheric pressure. The 0.15-GPa data of Hochheimer *et al.*<sup>10</sup> at 100 K show, however, a line shape similar to our results. In these data a small structure extends to lower frequencies.

In Fig. 5 we present finally the results for CuI. In agreement with the experimental data of Burns *et al.*<sup>15</sup> we find a broad TO peak with a small shoulder at the low-frequency side.

Figures 6–8 show the self-energies of the TO phonons in CuCl, CuBr, and CuI, respectively. The calculations have been carried out for small but finite wave vectors in the three main symmetry directions (100), (110), and (111). The results for the three different crystal orientations show small variations of the phonon self-energies due to the directional dependence of the eigenvectors of the TO

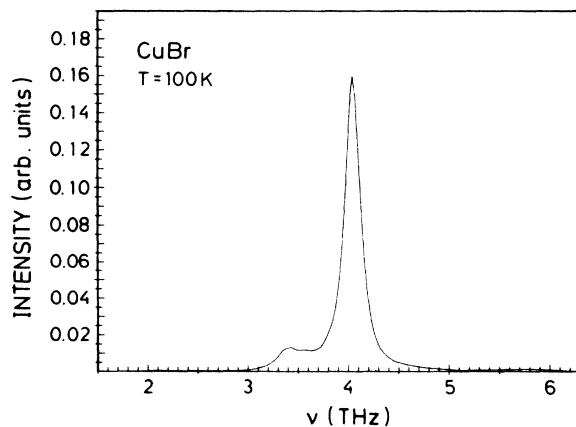


FIG. 4. Line shape of the  $\text{TO}(\Gamma)$  phonon in CuBr at 100 K calculated with the VOSM. Anharmonic parameters are  $\lambda' = 16e^2/r_0v_a$ ,  $\Delta_0 = 0.1$  THz.

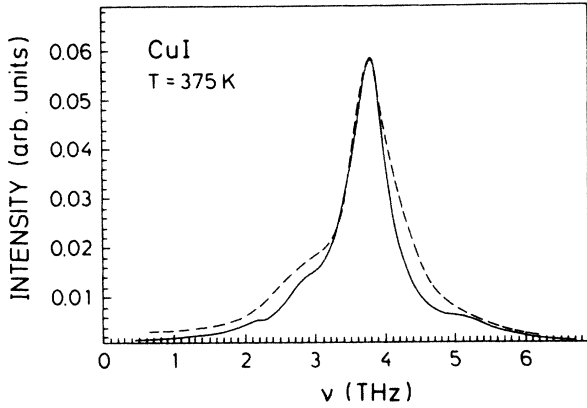


FIG. 5. Line shape of the  $\text{TO}(\Gamma)$  phonon in  $\text{CuI}$  at 375 K calculated with the VOSM (solid curve). The dashed curve shows the experimental spectrum of Burns *et al.* (Ref. 15). Anharmonic parameters are  $\lambda' = 28e^2/r_0v_a$ ,  $\Delta_0 = 0.6$  THz.

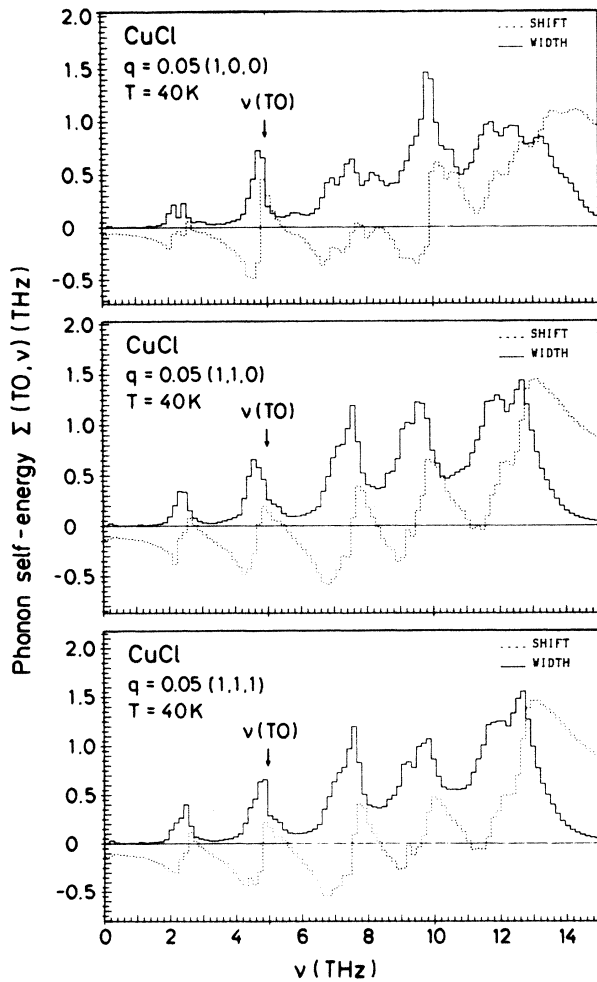


FIG. 6. Self-energies of the  $\text{TO}(\Gamma)$  phonon in  $\text{CuCl}$  at 40 K calculated with the VSM for small finite wave vectors  $q$  in the main symmetry directions. The solid and dashed lines represent the damping  $\Gamma$  and the shift  $\Delta$ , respectively. The frequency of the quasi-harmonic  $\text{TO}(\Gamma)$  mode is indicated by arrows.

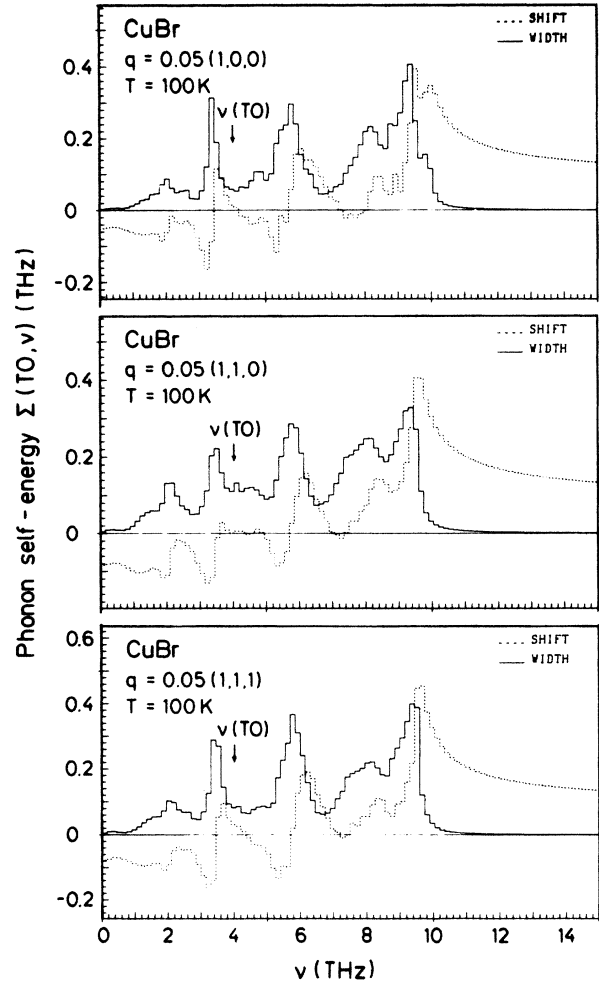


FIG. 7. Self-energies of the  $\text{TO}(\Gamma)$  phonon in  $\text{CuBr}$  at 100 K. The notation is as in Fig. 6.

phonon even at very small wavevectors. The overall shape of the frequency shift  $\Delta(\nu)$  (dashed line) and the damping  $\Gamma(\nu)$  (solid line) is, however, the same for all three orientations. We now focus on Fig. 6(a) and discuss the relation between the self-energy and line shape of the  $\text{TO}(\Gamma)$  phonon in a Fermi resonance [Eq. (11)]. The largest contributions to the line shape arise from the structures in the self-energy at frequencies which are close to the frequency of the  $\text{TO}(\Gamma)$  phonon (indicated by the arrow). Real and imaginary parts of the self-energy are related by the Kramers-Kronig relation. Thus a peak in the damping corresponds to a step rise of the shift function  $\Delta(\omega)$  from negative values below the resonance to positive values above the resonance with a zero shift at the resonance. For simplicity we discuss first the case in which the frequency of the  $\text{TO}(\Gamma)$  mode  $\omega(\text{TO}) = \omega_{\text{TO}}$  coincides with the peak position of the damping function. In this case  $\Delta(\text{TO}, \omega_{\text{TO}})$  is equal to zero. Thus the function  $[\omega(\text{TO}) + \Delta(\text{TO}, \omega) - \omega]^{-2}$  has singularities at  $\omega_0 = \omega(\text{TO})$ , at  $\omega_- = \omega(\text{TO}) + \Delta(\text{TO}, \omega_-)$ , and at  $\omega_+ = \omega(\text{TO}) + \Delta(\text{TO}, \omega_+)$ . This gives rise to two peaks in the line shape of the  $\text{TO}(\Gamma)$  phonon at  $\omega_-$  and  $\omega_+$ , since there the damping  $\Gamma(\text{TO}, \omega)$  is already small. There is, in principle,

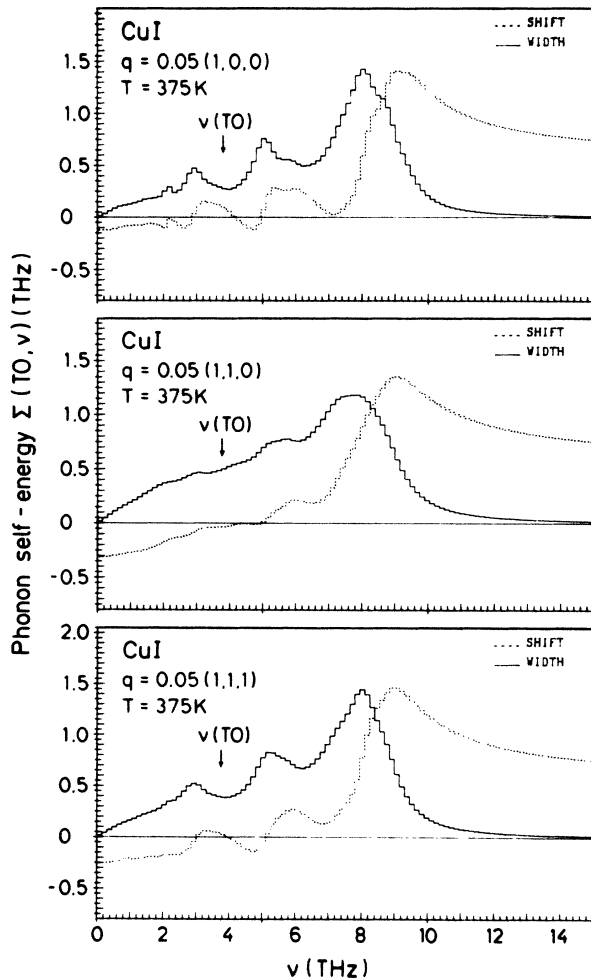


FIG. 8. Self-energies of the  $\text{TO}(\Gamma)$  phonon in CuI at 375 K. The notation is as in Fig. 6.

always a third peak at  $\omega_0$  which is, however, strongly broadened due to the maximum of  $\Gamma(\text{TO}, \omega)$  at  $\omega_0$ . A very similar behavior is obtained when the maximum of the damping function is shifted slightly away from the frequency  $\omega_{\text{TO}}(\Gamma)$ . In this case  $\omega_0$  is shifted away from the maximum of the damping and becomes therefore more pronounced. This leads also to asymmetries and differences in the intensities and widths of the two peaks at  $\omega_+$  and  $\omega_-$ . The preceding discussion shows that the small third peak in the spectrum of CuCl reported in Fig. 3 and observed in some of the experimental data is an intrinsic property of the Fermi resonance.

When the  $\text{TO}(\Gamma)$  frequency is separated still further from the resonance in the self-energy, the  $\omega_0$  resonance is strongly enhanced and one or the other or both of the side peaks at  $\omega_+$  and  $\omega_-$  may disappear. This disappearance depends on the detailed behavior of  $\Delta(\text{TO}, \omega)$ . In CuBr and CuI the upper side peak disappears and the lower peak is broadened due to the strong damping at  $\omega_-$ .

In order to analyze our results further, we show in Figs. 9–11 the two-phonon sum and difference bands for the three copper halides. The  $\text{TO}(\Gamma)$  frequencies are indicat-

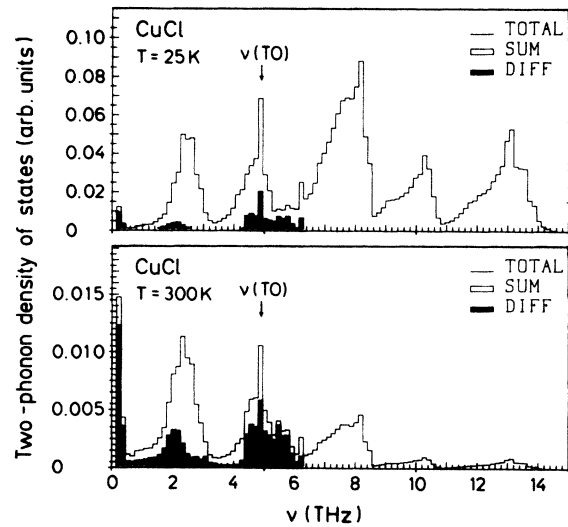


FIG. 9. Two-phonon densities of states of CuCl at 25 and 300 K. The outlines represent the total density of the difference (black areas) and the summation (blank areas) densities. The arrows indicate the quasi-harmonic  $\text{TO}(\Gamma)$  frequency.

ed by arrows. In CuCl the  $\text{TO}(\Gamma)$  frequency lies at the cutoff of a strong  $\text{TA}(X) + \text{LA}(X)$  combination band. Additional contributions due to  $\text{TO}(X) - \text{TA}(X)$  difference bands are small but still important at 40 K. This situation gives rise to a pronounced double-peak structure in the line shape of the  $\text{TO}(\Gamma)$  phonon (Figs. 2 and 3).

In CuBr the frequency of the  $\text{TO}(\Gamma)$  phonon has moved out of a strong  $\text{LO}(X) - \text{TA}(X)$  difference band. The line shape (Fig. 4) shows, therefore, a relatively sharp peak at about the  $\text{TO}(\Gamma)$  frequency of the quasi-harmonic phonon. This peak exhibits, however, a strong shoulder at the low-frequency side. Since this shoulder is essentially due

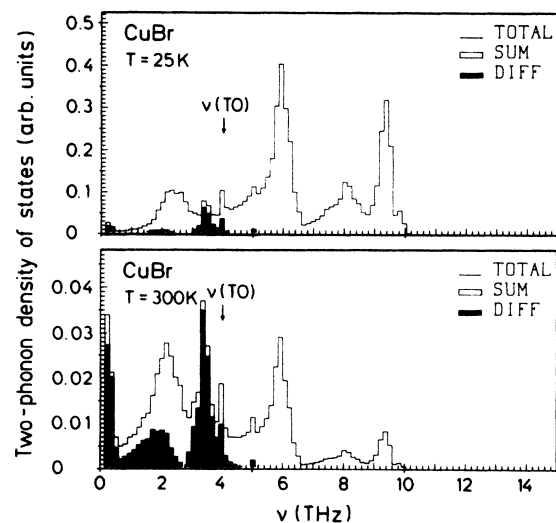


FIG. 10. Two-phonon densities of states of CuBr at 25 and 300 K. The notation is as in Fig. 9.

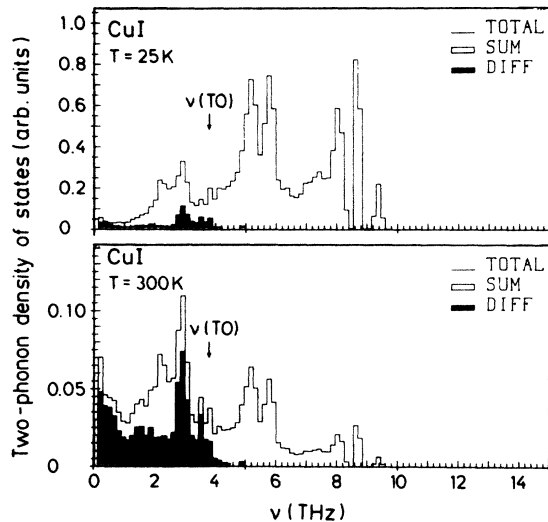


FIG. 11. Two-phonon densities of states of CuI at 25 and 300 K. The notation is as in Fig. 9.

to difference processes, it disappears rapidly with decreasing temperature. This temperature behavior is confirmed by the experimental results of Hochheimer *et al.*<sup>10</sup> In CuI the situation is similar to that in CuBr. Here the frequency difference between the  $LO(X)-TA(X)$  difference band and the  $TO(\Gamma)$  mode is even larger than in CuBr. The  $TO(\Gamma)$  line shape is therefore again dominated by a strong peak at about the frequency of the quasiharmonic

$TO(\Gamma)$  phonon. At low temperatures this peak is rather sharp. Its line width increases rapidly with increasing temperature due to the population of the difference bands. At the same time a shoulder is build up at the low-frequency side. This behavior is in agreement with the measured spectra of Burns *et al.*<sup>15</sup>

#### IV. CONCLUSIONS

We have shown that the observed line shapes of the  $TO(\Gamma)$  phonon in CuCl, CuBr, and CuI can be calculated on the basis of a lattice-dynamical model, which reproduces the measured phonon dispersion curves and gives the appropriate two-phonon summation and difference bands. Our results show that the three-phonon interactions give rise to Fermi resonances, which determine the line shapes of the  $TO(\Gamma)$  phonons. The anharmonic three-phonon interaction can be taken into account in a leading term approximation, in which only the third-order terms due to the nearest-neighbor bond-stretching interaction are taken into account. Our results show that there is no need to consider vertex renormalizations by two-phonon bound or resonance states. It seems more important to determine the self-energies self-consistently by taking into account the line width and the quasiharmonic shifts of the phonons involved in the diagrammatic expansion of the self-energy. Our results show clearly that the anomalous line shapes of the copper halides are caused by Fermi resonances and that there is no need to consider off-center positions of the  $Cu^+$  ions. We therefore conclude that the defect model of Vardeny *et al.*<sup>13</sup> does not correctly describe the origin of these anomalies.

\*Permanent address: Physics Department, University of Thessaloniki, Thessaloniki, Greece.

<sup>1</sup>M. Krauzman, in *Light Scattering Spectra of Solids*, edited by G. B. Wright (Springer-Verlag, Berlin, 1969), p. 109.

<sup>2</sup>M. A. Nusimovici and A. Meskini, *Phys. Status Solidi B* **52**, K62 (1972).

<sup>3</sup>T. Fukumoto, K. Tabuchi, S. Nakashima, and A. Mitsuishi, *J. Phys. Soc. Jpn.* **35**, 622 (1973).

<sup>4</sup>B. Prevot and M. Sieskind, *Phys. Status Solidi B* **59**, 133 (1973).

<sup>5</sup>J. E. Potts, R. C. Hanson, C. T. Walker, and C. Schwab, *Phys. Rev. B* **9**, 2711 (1974).

<sup>6</sup>I. P. Kaminow and E. H. Turner, *Phys. Rev. B* **5**, 1564 (1972).

<sup>7</sup>M. L. Shand, L. Y. Ching, and E. Burstein, *Solid State Commun.* **15**, 1209 (1974).

<sup>8</sup>M. Krauzman, R. M. Pick, H. Poulet, G. Hamel, and B. Prevot, *Phys. Rev. Lett.* **33**, 528 (1974).

<sup>9</sup>T. Fukumoto, S. Nakashima, K. Tabuchi, and A. Mitsuishi, *Phys. Status Solidi B* **73**, 341 (1976).

<sup>10</sup>H. D. Hochheimer, M. L. Shand, J. E. Potts, R. C. Hanson, and C. T. Walker, *Phys. Rev. B* **14**, 4630 (1976).

<sup>11</sup>A. Blacha, Ph.D. thesis, University of Stuttgart, 1985 (unpublished).

<sup>12</sup>A. Blacha, G. Kourouklis, and M. Cardona (unpublished).

<sup>13</sup>Z. Vardeny and O. Brafman, *Phys. Rev. B* **19**, 3276 (1979).

<sup>14</sup>B. Hennion, B. Prevot, M. Krauzman, R. M. Pick, and B. Dorner, *J. Phys. C* **12**, 1609 (1979).

<sup>15</sup>G. Burns, I. H. Dacol, M. W. Shafer, and R. Albey, *Solid State Commun.* **24**, 753 (1974).

<sup>16</sup>J. Ruvalds and A. Zawadowski, *Phys. Rev. B* **2**, 1172 (1970).

<sup>17</sup>M. L. Shand, H. D. Hochheimer, M. Krauzman, J. E. Potts, R. G. Hanson, and C. T. Walker, *Phys. Rev. B* **14**, 4637 (1976).

<sup>18</sup>G. Kanellis, W. Kress, and H. Bilz, *Phys. Rev. B* **33**, xxxx (1986).

<sup>19</sup>A. A. Maradudin and A. E. Fein, *Phys. Rev.* **128**, 2589 (1962).

<sup>20</sup>J. Oitmaa, *Aust. J. Phys.* **20**, 495 (1967).

<sup>21</sup>H. Bilz and W. Kress, *Phonon Dispersion Relations in Insulators* (Springer-Verlag, Berlin, 1979).

<sup>22</sup>R. Migoni, Ph.D. thesis, University of Stuttgart, 1976 (unpublished).

<sup>23</sup>R. Migoni, H. Bilz, and D. Bäuerle, *Phys. Rev. Lett.* **37**, 1155 (1976).

<sup>24</sup>K. Fischer, *Phys. Status Solidi B* **66**, 449 (1974).